Synthesis and Characterization of Poly(benzobisoxazole)s and Poly(benzobisthiazole)s with 2,2′-Bipyridyl Units in the Backbone

Sze Chit Yu, Xiong Gong, and Wai Kin Chan*

Department of Chemistry, University of Hong Kong, Pokfulam Road, Hong Kong

Received March 11, 1998; Revised Manuscript Received May 26, 1998

ABSTRACT: This paper reports the synthesis and physical properties of a series of novel bipyridine-containing poly(benzobisoxazole)s and poly(benzobisthiazole)s. The polymers were synthesized by polycondensation of 2,2′-bipyridine-5,5′-dicarboxylic acid with diaminobenzenediols in poly(phosphoric acid). Some model compounds were also synthesized by a similar approach for comparison. The polymers exhibited extremely high thermal stabilities in air or nitrogen atmosphere. From the polarized microscopic studies, lyotropic mesophases were observed in some polymer solutions in methanesulfonic acid. The 2,2′-bipyridyl moieties on the polymer main chain were able to form metal complexes with bis(2,2′-bipyridyl)ruthenium(II) compounds, which was proved by different characterization methods such as electronic and luminescence spectroscopy, cyclic voltammetry, and thermal analysis. The charge carriers mobilities of the polymer metal complexes are of the order of 10^{-5} cm^2 V^{-1} s^{-1}, which are 2 orders of magnitude higher than that of the metal-free polymers. This clearly shows that the ruthenium complexes can play the role as charge carriers in the charge transport process.

Introduction

In recent years, the development of aromatic conjugated polymers has been a topic of interest because of their potentials for technological applications ranging from structural to electronic and nonlinear optical properties.[1] Poly(benzobisoxazole)s (PBOs) and poly(benzobisthiazole)s (PBTs) comprise a class of heterocyclic polymers which exhibit excellent thermal and oxidative stability and good solvent resistance.[2] The high degree of molecular rigidity in the polymer backbone and the intermolecular interaction give rise to high modulus polymers. Fibers drawn from these polymer solutions have extremely high tensile strength and tensile modulus. Substantial effort has been expended in attempts to improve the fiber strengths. On the other hand, the photophysical and photochemical properties of these polymers are also of considerable interest due to the potential applications in optoelectronic devices.[3−5] The nonlinear optical,[4] luminescence,[5] and electrical conducting[6] properties of some benzoazole-typed polymers have been reported.

Recently, we reported the synthesis of some rigid-rod polymers which contain different types of ruthenium polypyridine complexes in the polymer main chain.[7] It was found that the ruthenium complexes can act as photosensitizers, which was demonstrated by the enhancement in photoconductivity at the region where the metal-free conjugated polymers do not absorb. In addition, the charge carrier mobilities also changed after the incorporation of metal complexes. Tris(2,2′-bipyridyl)ruthenium(II), $[Ru(bpy)_3]^{2+}$, complex and its derivatives have attracted the attention of many researchers because of the unique combination of chemical stability, redox properties, excited-state reactivity, luminescence emission, and excited-state lifetimes.[8] They have demonstrated promising potential applications in solar energy conversion, polymer supported electrodes, photosensitizers, emission sensitizers, photogalvanic cells, and electroluminescence.[9] In the literature, there are several examples of conjugated polymers which contain the 2,2′-bipyridyl moiety in the polymer main chain. Different properties such as photorefractivity,[10] metal ion sensing,[11] catalytic activities, and electrical conductivities[12] have been investigated.

In this paper, we report the synthesis and characterization of a series of poly(benzobisoxazoles) and poly(benzobisthiazole)s which contain the 2,2′-bipyridyl moiety. By incorporation of the bipyridine unit in the polymer, the rigidity of the backbone and the extended π-conjugation are retained. The polymers are capable of forming macromolecular transition metal complexes which give rise to very interesting photonic and electrochemical properties. It is also commonly known that ruthenium polypyridine complexes exhibit several reversible metal- or ligand-centered redox processes, which may facilitate charge transport in the polymer. This paper reports the synthesis and metal complex formation properties of these polymers and the corresponding model compounds.

Experimental Section

Materials. Phosphorus pentoxide, phosphoric acid, 2-aminophenol, and 2-aminothiophenol were purchased from Lancaster Synthesis Ltd. and were used as received. NMP was distilled over calcium hydride under reduced pressure. 2,2′-Bipyridine-5,5′-dicarboxylic acid (**3**),[13] 2,2′-bipyridine-4,4′-dicarboxylic acid (**4**), 4,6-diamino-1,3-benzenediol dihydrochloride (**5**),[14] 2,5-diamino-1,4-benzenediol dihydrochloride (**6a**), 2,5-diamino-1,4-benzenedithiol dihydrochloride (**6b**),[15] and *cis*-dichlorobis(2,2′-bipyridine)ruthenium(II) dihydrate,[16] [$Ru(bpy)_2Cl_2 \cdot 2H_2O$], were prepared according to the literature procedures.

Instruments. ^{1}H and ^{13}C NMR spectra were collected on a Bruker 300 DPX NMR spectrometer. FTIR spectra (KBr pellet) were collected on a Bio-Rad FTS-7 FTIR spectrometer. Mass spectrometry was performed on a high-resolution Finnigan MAT-95 mass spectrometer. Thermal analyses were performed on a Perkin-Elmer DSC7 and TGA7 thermal analyzer with a heating rate of 10 and 15 °C/min, respectively. The excitation and emission spectra were collected on a SPEX 1681 Fluorolog-2 spectrofluorometer. The polarized microscope observation was performed on a Leica DMR microscope equipped with a Leitz microscope heater. The viscosity measurements were performed in a constant-temperature bath

S0024-9297(98)00381-7 CCC: $15.00
Published on Web 08/08/1998

(30 °C) using an Ubbelohde viscometer, with the solution concentration of 0.5 g/dL in methanesulfonic acid. Cyclic voltammetry measurements on polymers and model compounds were performed on a Princeton Applied Research 270 potentiostat with a glassy carbon working electrode and silver/silver chloride reference electrode. Distilled acetonitrile was used as the solvent and tetrabutylammonium hexafluorophosphate as the supporting electrolyte. Small amount of ferrocene was added as an internal standard.

Synthesis of Polymers. The synthesis of polymer **1a** using the diacid as the monomer is described as the general procedure. 2,5-Diamino-1,4-benzenediol dihydrochloride (**5**) (0.38 g, 1.78 mmol) was added to a freshly prepared poly(phosphoric acid) solution (75% P_2O_5). The mixture was stirred at 80 °C for 24 h under nitrogen and 24 h under reduced pressure until no more gas bubbles were evolved. 2,2′-Bipyridine-5,5′-dicarboxylic acid (**3**) (0.44 g, 1.78 mmol) and phosphorus pentoxide (10 g) were then added to the reaction mixture. The resulting slurry (83% P_2O_5 content with 3 wt % of polymer) was heated at 150 °C for 24 h, 160 °C for 24 h, 185 °C for 24 h, and then 195 °C for 24 h. The polymers solution was poured into hot water, and the solid was filtered off and washed with aqueous NaOH solution (5%). The polymer was finally purified by washing with water in a Soxhlet extractor for 2 days.

Synthesis of Model Compounds. The synthesis of model compound **7a** is described as the general procedure. Under a nitrogen atmosphere, a mixture of **3** (0.30 g, 1.2 mmol), 2-aminophenol (0.29 g, 2.7 mmol), and freshly prepared polyphosphoric acid (75%) was heated in stages to 180 °C for 24 h. After cooling, the solution was poured into hot water with stirring. The precipitate was purified by stirring with hot potassium carbonate solution and recrystallized from DMF. The product was dried under reduced pressure at 100 °C for 24 h and collected as light yellow powder (87% yield). Mp: 413 °C (dec). IR (KBr): ν = 1654, 1596, 744 cm^{-1}. ^{1}H NMR (CF_3COOH (TFA)−$CDCl_3$): δ 9.86 (d, J = 1.8 Hz, 2H), 9.33 (dd, J = 2.0, 8.5 Hz, 2H), 8.90 (d, J = 8.5 Hz, 2H), 8.01 (d, J = 7.4 Hz, 2H), 7.89 (d, J = 7.7 Hz, 2H), 7.78−7.67 (m, 4H). ^{13}C NMR (TFA−$CDCl_3$): δ 158.4, 150.9, 148.1, 146.3, 142.7, 136.9, 129.9, 128.3, 125.8, 124.9, 119.5, 112.5. MS: *m/e* 390.111 676; $C_{24}H_{14}N_4O_2$ requires *m/e* 390.111 676.

Model Compound 7b. The product was collected as light green solid (90% yield). Mp: 380 °C. IR (KBr): ν = 1655, 1588, 746 cm^{-1}. ^{1}H NMR (TFA−$CDCl_3$): δ 9.72 (s, 2H), 9.16 (d, J = 7.7 Hz, 2H), 8.91 (d, J = 7.9 Hz, 2H), 8.29 (m, 4H), 8.00−7.89 (m, 4H). ^{13}C NMR (TFA−$CDCl_3$): δ 165.6, 148.7, 146.1, 145.4, 143.3, 132.7, 131.5, 130.5, 129.8, 125.4, 123.7, 120.7. MS: *m/e* 422.065 992; $C_{24}H_{14}N_4S_2$ requires *m/e* 422.065 991.

Model Compound 7c. The product was collected as light brown solid (89% yield). Mp: 354 °C. IR (KBr): ν = 1654, 1593, 761 cm^{-1}. ^{1}H NMR (TFA−$CDCl_3$): δ 9.65 (s, 2H), 9.24 (d, J = 5.6 Hz, 2H), 8.76 (dd, J = 1.3, 5.6 Hz, 2H), 8.09 (d, J = 7.5 Hz, 2H), 7.91 (d, J = 8.0 Hz, 2H), 7.81−7.69 (m, 4H). ^{13}C NMR (TFA−$CDCl_3$): δ 158.5, 151.3, 148.0, 147.3, 139.7, 138.1, 130.1, 128.0, 125.7, 125.0, 121.6. MS: *m/e* 390.111 679, $C_{24}H_{14}N_4O_2$ requires *m/e* 390.111 676.

Model Compound 7d. The product was collected as light green solid (89% yield). Mp: 318 °C. IR (KBr): ν = 1654, 1587, 764 cm^{-1}. ^{1}H NMR (TFA−$CDCl_3$): δ 9.56 (s, 2H), 9.26 (d, J = 5.6 Hz, 2H), 8.55 (dd, J = 1.0, 5.6 Hz, 2H), 8.41 (d, J = 8.2 Hz, 2H), 8.30 (d, J = 8.0 Hz, 2H), 8.03−7.91 (m, 4H). ^{13}C NMR (TFA−$CDCl_3$): δ 166.0, 148.6, 147.6, 142.2, 133.1, 131.5, 130.1, 126.5, 123.4, 121.7, 120.8. MS: *m/e* 422.065 992, $C_{24}H_{14}N_4S_2$ requires *m/e* 422.065 991.

Synthesis of the Model Metal Complexes 8a-d. The synthesis of complex **8a** is described as the general procedure. Under a nitrogen atmosphere, silver trifluoromethanesulfonate (0.51 g, 2 mmol) was added to a solution of $Ru(bpy)_2Cl_2 \cdot 2H_2O$ (0.52 g, 1 mmol) in acetone (100 mL). The solution was stirred at room temperature for 2 h. After filtration with a pad of Celite, the filtrate was evaporated to dryness to give $Ru(bpy)_2(acetone)_2(OTf)_2$ (0.72 g, 90% yield). The triflate salt was added to a solution of **7a** (0.36 g, 0.90 mmol) in NMP (25 mL), and the solution was heated at 120 °C for 48 h. After cooling, an aqueous solution of KPF_6 was added and the precipitate was collected by filtration. The resulting solid was washed with methanol thoroughly and dried under reduced pressure at 100 °C for 1 day. Yield: 78%. Mp: 395 °C (dec). IR (KBr): ν = 1653, 1604, 764, 840 cm^{-1}. ^{1}H NMR (DMSO-d_6): δ 9.56 (s, 2H), 9.26 (d, J = 5.6 Hz, 2H), 8.55 (dd, J = 1.0, 5.6 Hz, 2H), 8.41 (d, J = 8.2 Hz, 2H), 8.30 (d, J = 8.0 Hz, 2H), 8.03−7.91 (m, 4H). ^{13}C NMR (DMSO-d_6): δ 166.0, 148.6, 147.6, 142.2, 133.1, 131.5, 130.1, 126.5, 123.4, 121.7, 120.8. FABMS: *m/e* 949 ($M^+ - PF_6$); $C_{44}H_{30}N_8O_2PF_6Ru$ requires *m/e* 948.8.

Complex 8b. Yield: 80%. Mp: 369 °C (dec). IR (KBr): ν = 1657, 1602, 765, 841 cm^{-1}. ^{1}H NMR (DMSO-d_6): δ 9.15 (d, J = 8.6 Hz, 2H), 8.95 (d, J = 8.2 Hz, 2H), 8.90−8.84 (m, 4H), 8.37−8.32 (m, 4H), 8.20 (t, J = 7.6 Hz, 2H), 8.02 (d, J = 5.3 Hz, 2H), 7.89 (d, J = 5.1 Hz, 2H), 7.83−7.76 (m, 4H), 7.56−7.43 (m, 6H). ^{13}C NMR (DMSO-d_6): δ 158.0, 157.5, 156.7, 156.2, 152.0, 151.4, 150.1, 149.2, 140.8, 138.3, 138.1, 135.4, 128.0, 127.9, 126.8, 126.4, 125.5, 124.7, 124.6, 124.4, 120.3, 111.1. FABMS: *m/e* 981 ($M^+ - PF_6$); $C_{44}H_{30}N_8S_2PF_6Ru$ requires *m/e* 980.9.

Complex 8c. Yield: 77%. Mp: 370 °C (dec). IR (KBr): ν = 1654, 1603, 844 cm^{-1}. ^{1}H NMR (DMSO-d_6): δ 9.77 (s, 2H), 8.91 (dd, J = 3.7, 8.2 Hz, 4H), 8.24 (m, 6H), 8.07 (d, J = 6.0 Hz, 2H), 7.99 (t, J = 8.4 Hz, 4H), 7.91 (d, J = 5.3 Hz, 2H), 7.77 (d, J = 5.2 Hz, 2H), 7.64−7.53 (m, 8H). ^{13}C NMR (DMSO-d_6): δ 159.1, 157.4, 156.3, 156.2, 152.3, 151.6, 151.0, 150.5, 141.1, 138.3, 134.3, 127.9, 127.2, 125.7, 124.8, 124.5, 122.1, 120.6, 111.4. FABMS: *m/e* 949 ($M^+ - PF_6$); $C_{44}H_{30}N_8O_2PF_6$-Ru requires *m/e* 948.8.

Complex 8d. Yield: 81%. Mp: 349 °C (dec). IR (KBr): ν = 1653, 1602, 849 cm^{-1}. ^{1}H NMR (DMSO-d_6): δ 9.56 (s, 2H), 8.87 (d, J = 5.1 Hz, 4H), 8.31−8.13 (m, 10 H), 7.94 (d, J = 6.0 Hz, 2H), 7.91 (d, J = 5.1 Hz, 2H), 7.74 (d, J = 5.1 Hz, 2H), 7.68−7.51 (m, 8H). ^{13}C NMR (DMSO-d_6): δ 163.2, 157.3, 156.3, 153.3, 152.1, 151.6, 151.0, 140.4, 138.2, 135.4, 128.0, 127.4, 126.9, 125.2, 124.5, 123.7, 122.9, 121.9. FABMS: *m/e* 981 ($M^+ - PF_6$); $C_{44}H_{30}N_8S_2PF_6Ru$ requires *m/e* 980.9.

Synthesis of Polymer Metal Complexes. The preparation of the polymer metal complex **Ru−1b** is described as the general procedure. Under a nitrogen atmosphere, a mixture of $Ru(bpy)_2(acetone)_2(OTf)_2$ (0.36 g, 0.45 mmol), polymer **1b** (0.14 g, 0.45 mmol calculated by the molecular weight of the repeating unit), and NMP (25 mL) was stirred at 120 °C for 48 h. The dark red solution became homogeneous during the course of the reaction. The reaction mixture was cooled and precipitated in an excess of aqueous KPF_6 solution. The polymer obtained was washed thoroughly with water and methanol, and the product was collected as a reddish brown powder.

Physical Characterizations. The polymer film was prepared by casting a polymer solution (6 mg/mL) onto an ITO glass, and the solvent was evaporated slowly. The typical thickness of the polymer film was approximately 1 μm. For the metal-containing polymers, a mixture of acetonitrile/DMF was used as the solvent. The charge carrier mobilities were determined by the conventional time-of-flight experiment.[17] A thin layer of gold electrode (120 Å) was coated on the polymer film surface by sputtering. A Laser Science VSL-337 nitrogen laser was used to generate a pulsed laser source [wavelength = 337.1 nm, pulse energy = 120 μJ, and pulse full width at half-maximum (FWHM) = 3 ns].

Results and Discussion

Synthesis of Polymers, Model Compounds, and Polymer Metal Complexes. All polymerization reactions were carried out in freshly prepared poly(phosphoric acid) (PPA). PPA was prepared by adding an appropriate amount of phosphorus pentoxide to phosphoric acid and then heating at 150 °C under nitrogen for 24 h. In the polymerization reaction, the PPA served as a solvent, catalyst, and dehydrating agent. Hydrogen chloride was first completely removed from the reaction

Scheme 1

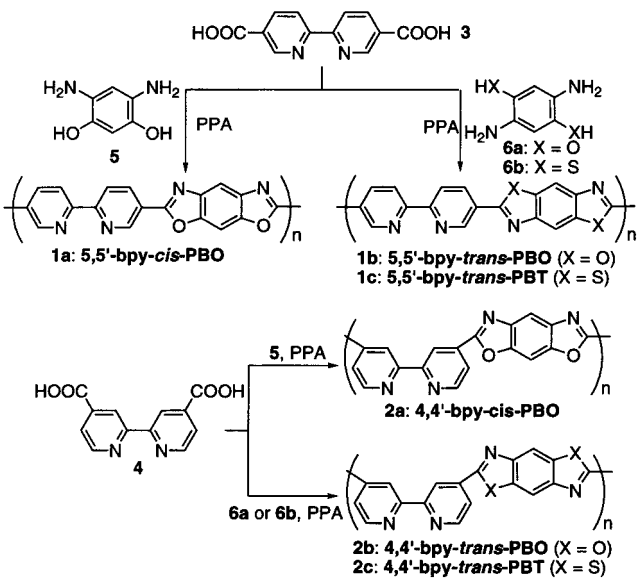

mixture of diaminobenzenediol dihydrochloride in PPA before the addition of 2,2′-bipyridine-5,5′-dicarboxylic acid. Solid P_2O_5 was then added according to the P_2O_5 content adjustment method.[2a] After the monomers were mixed at 90 °C, the polymerization was carried out at a temperature above 150 °C. This procedure gave polymers with inherent viscosity in the range of 2−5 dL/g measured in methanesulfonic acid (MSA) solution at 30 °C. We also tried to use 2,2′-bipyridine-5,5′-dicarbonyl chloride as the monomer, and the resulting polymers only showed a slight increase in viscosity (Scheme 1).

All the 5,5′-substituted PBO and PBT (**1a**−**c**) are soluble in MSA, concentrated H_2SO_4, trifluoroacetic acid (TFA), formic acid, and nitromethane/$AlCl_3$ mixture. They can form a good quality film by casting the polymer solution on an indium tin oxide (ITO) glass surface. However, the 4,4′-substituted polymers (**2a**−**c**) are only soluble in MSA and nitromethane/$AlCl_3$ and their film quality is relatively poor. Therefore, most of the physical measurement were carried out on polymers **1a**−**c** and their metal complexes.

To order to study the optimum condition for the metal complex formation and structural characterization, model compounds **7a**−**d** were synthesized (Scheme 2). They were prepared by the same procedure as the polymerization reaction using 2-aminophenol and 2-aminothiophenol as the starting materials. All model compounds were obtained in high yield, and their structures were studied by different spectroscopic techniques. It was found that direct complexation of the model compounds with *cis*-$Ru(bpy)_2Cl_2 \cdot 2H_2O$ in DMF at high-temperature failed to give the desired metal complex. A more efficient alternative procedure was used instead.[16] The ruthenium acetone complex was first synthesized by reaction between $Ru(bpy)_2Cl_2 \cdot 2H_2O$ and silver triflate (Scheme 3). The ruthenium triflate salt then reacted with 1 equiv of the bipyridine ligand (N−N), and the metal complex was isolated as the hexafluorophosphate salt. All of the model metal complexes **8a**−**d** were obtained in high yield. Similar procedure was used to prepare the polymer metal complexes (Scheme 4). From the elemental analysis results, the ruthenium contents in **Ru**−**1a**−**c** and **Ru**−**2a**−**c** are approximately 0.2−0.7 per unit of bipyridyl group and the 5,5′-substituted polymers have significantly higher metal content (Table 3). The metal content in the polymers may also affect the solubility of the polymer metal complexes. It was observed that, after the metal complex formation, **Ru**−**1a**−**c** became very soluble in polar aprotic solvents such as DMF, NMP, and DMSO due to the formation of the positively charged $Ru(bpy)_3^{2+}$-typed species on the polymer main chain. On the other hand, **Ru**−**2a**−**c** are only partly soluble in these solvent probably due to the lower metal content in the polymer main chain.

Table 1. Syntheses and Properties of Polymers 1a−c and 2a−c

		T_d (°C)[b]			
polymer	yield (%)[a]	in air	in N_2	η_{inh} (dL/g)[c]	$\lambda_{max,abs}$ (nm)
1a	90	657	691	5.2	408, 430
1b	82	591	668	3.1	406
1c	83	537	585	3.7	398
2a	87	608	668	2.1	348
2b	86	586	648	1.7	372
2c	87	569	597	2.1	378

[a] Percentage yield after purification. [b] Decomposition temperature determined by TGA. [c] Inherent viscosity measured in methanesulfonic acid at 30 °C with $c = 0.25$ g/dL.

Structural Characterization. In the FTIR spectra, polymer **1b** and its corresponding ruthenium complex **Ru**−**1b** both exhibit a characteristic pyridine ring C=N stretching at 1600 cm^{-1}. All polymers also show a C=N stretching band due to the oxazole or thiazole ring systems at 1650 cm^{-1}. Another absorption band at 850

Scheme 2

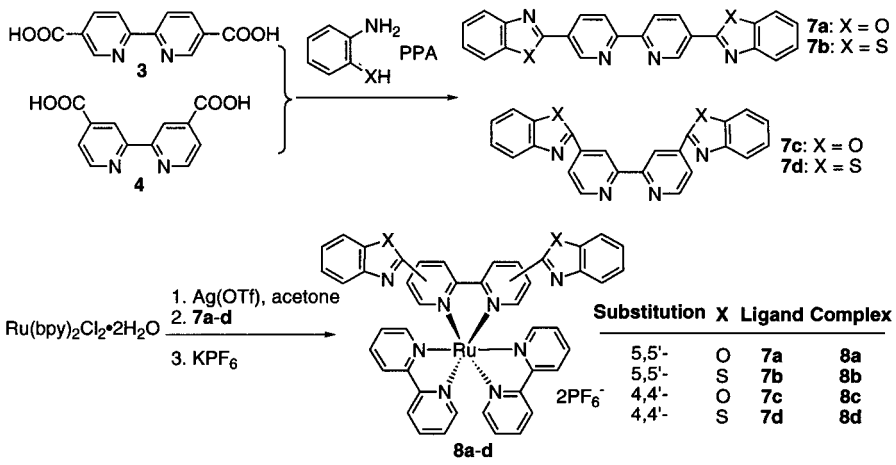

Table 2. Properties of Model Compounds

compd	yield (%)	T_d[a] (°C)	$\lambda_{max,abs}$ (nm)	ϵ_{max} (L mol^{-1} cm^{-1})	$E_{1/2}$(ox), V vs Ag/AgCl	$E_{1/2}$(red), V vs Ag/AgCl
7a	87	413	382	47 300		
7b	90	404	384	59 000		
7c	89	374	296[b]	16 000		
			334	22 600		
7d	89	358	334	38 100		
8a	78	395	286	59 300	1.41	−0.78
			334[b]	32 800		−1.16
			374	53 700		−1.52
			396[b]	40 400		−1.77
			530	4 500		
8b	80	369	286	54 300	1.41	−0.81
			376	42 000		−1.14
			538	3 300		−1.51
						−1.74
8c	77	370	286	60 800	1.42	−0.94
			316	36 800		−1.39
			408	17 400		−1.55
			498	16 900		−1.81
8d	81	349	286	37 000	1.40	−0.96
			324	24 600		−1.35
			428	11 800		−1.54
			520	8 900		−1.74

[a] Decomposition temperature determined by TGA under N_2 atmosphere. [b] Approximate position; the peak appears as a shoulder.

Scheme 3

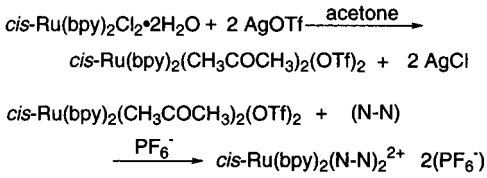

Scheme 4

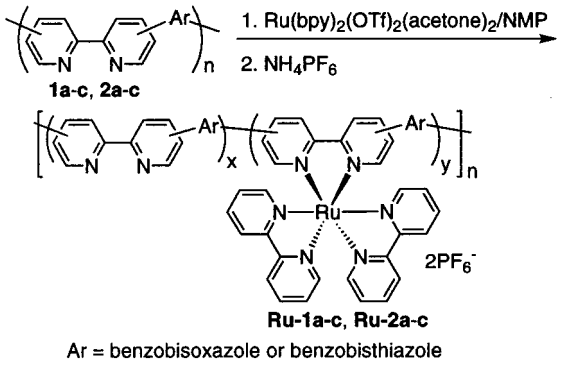

cm^{-1} is ascribed to the out-of-plane C−H bending of the tetrasubstituted benzobisoxazole moiety. After the incorporation of metal complex to the polymer main-chain, a very strong band is found at 840 cm^{-1} due to the P−F stretching of the counteranions.

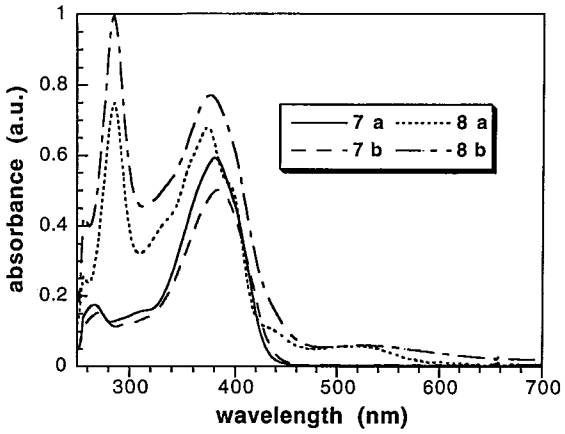

Figure 1. UV−vis spectra of the 5,5′-substituted model compounds **7a**,**b** and their corresponding ruthenium complexes **8a**,**b** in formic acid solution.

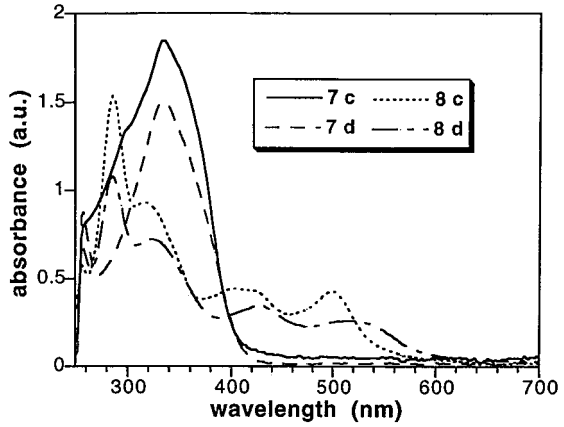

Figure 2. UV−vis spectra of the 4,4′-substituted model compounds **7c**,**d** and their corresponding ruthenium complexes **8c**,**d** in formic acid solution.

Figures 1 and 2 show the absorption spectra of the 5,5′- and 4,4′-substituted model compounds in formic acid solution, respectively. For other pyridine- or bipyridine-based polymers reported in the literature, formic acid was commonly used as the solvent for spectroscopic studies. The protonation of pyridine by formic acid was not observed due to its low acidity.[18] The absorption peak due to the $\pi-\pi^*$ transition for compounds **7a**,**b** is found at 384 nm. On the other hand, the same electronic transition for compounds **7c**,**d** appears at 334 nm. This is clearly due to the less extended π electrons delocalization in the 4,4′-substituted bipyridine ring systems. After the formation of metal complex, the $\pi-\pi^*$ electronic transitions in both **8a**,**b** show a significant blue shift (λ_{max} = 374 nm). Another very intense peak is also observed at 286 nm, which is attributed to the ligand-centered (LC) $\pi-\pi^*$

Table 3. Properties of Polymer Metal Complexes

complex	T_d (°C) in air	T_d (°C) in N_2	% wt. loss at 800 °C	Ru content (%)[a]	$\lambda_{max,abs}$ (nm)	μ_h (10^{-5} cm^2 V^{-1} s^{-1})[c]	μ_e (10^{-5} cm^2 V^{-1} s^{-1})[d]
Ru-1a	466	478	36	69	288, 408, 430, 480[b]		
Ru-1b	298	392	48	52	286, 406, 520[b]	1.4	3.5
Ru-1c	296	366	52	46	288, 398, 525[b]	4.0	7.1
Ru-2a	307	389	54	22	288, 352, 510[b]	*e*	*e*
Ru-2b	305	383	56	21	288, 370, 500	*e*	*e*
Ru-2c	305	385	52	30	288, 380, 500	*e*	*e*

[a] Percentage of bipyridyl unit functionalized with ruthenium complex. [b] Approximate position; the peak appears as a shoulder. [c] Hole carrier mobility measured at T = 298 K under an electric field of E = 32 kV/cm. [d] Electron carrier mobility measured at T = 298 K under an electric field of E = 18 kV/cm. [e] Not determined due to poor film quality.

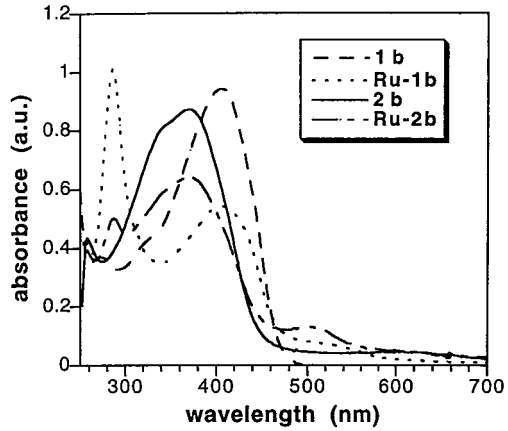

Figure 3. UV−vis spectra of **1b**, **2b**, **Ru**−**1b**, and **Ru**−**2b**.

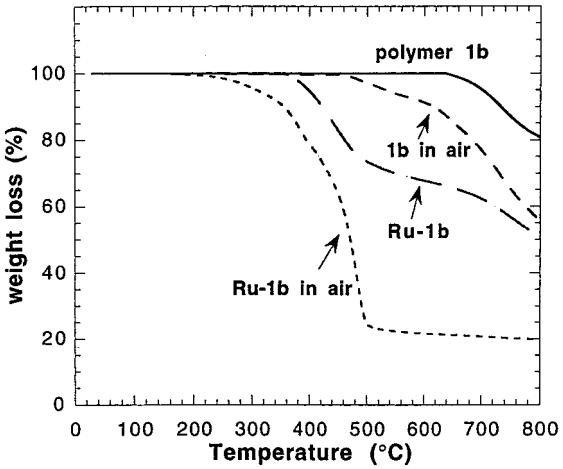

Figure 4. TGA thermograms of polymer **1b** and **Ru**−**1b** under nitrogen and air.

transition of the 2,2′-bipyridine ligand. In addition, the peak at 530 nm is assigned to the MLCT transition, which is a characteristic electronic transition in ruthenium polypyridine complexes. For compounds **8c**,**d**, similar spectral features are observed for the LC transitions. However, two well-separated MLCT bands have been observed at approximately 430 and 520 nm. The lower energy transition band corresponds to the promotion of an electron to the ligand which is easier to be reduced, i.e., ligand **7c** or **7d**. The detail spectroscopic data for these model compounds are summarized in Table 2.

For the polymers with ruthenium complexes, they have absorption features very similar to the corresponding model compounds. The UV−vis spectra of polymer **1b**, **2b**, and their metal complexes are shown in Figure 3. The peak due to the $\pi-\pi^*$ transition of the conjugated backbone shows a blue-shift because of the more extended π-conjugation in the polymers. For the polymer metal complexes **Ru**−**1b** and **Ru**−**2b**, the LC and MLCT bands can also be found at 288 and 510 nm, respectively. All this evidence shows the incorporation of ruthenium on the polymer main chain.

Thermal Properties. The TGA thermograms of polymer **1b** and **Ru**−**1b** are shown in Figure 4. All the PBO polymers demonstrate very high thermal stabilities (Table 1) which are comparable to other poly(benzobisazole)s reported in the literature. The PBO-type polymers are stable up to above 650 °C in nitrogen atmosphere and 590 °C in air. The decomposition temperatures of PBT-type polymers are lower than that of PBOs but are still stable up to 585 °C. After the formation of metal complexes, the thermal stability of the polymers decreases. The decomposition temperatures of the polymer metal complexes are quite similar to the model compounds **8a**−**d.** The decrease in thermal stability is probably due to the presence of the ruthenium bipyridine complexes which decompose first upon heating. Moreover, the packing between different polymer chains became less efficient after the incorporation of the bulky $Ru(bpy)_2$ moieties. As a result, the interaction between different molecules and, hence, the thermal stabilities are reduced. Similar trends can also be found in the model compounds. Model compounds **8a**−**d** exhibit lower thermal stability compared to the metal-free compounds **7a**−**d** (Table 2).

Figure 5. Optical micrograph of the lyotropic solution of polymer **1a** (6.3 wt %) in methanesulfonic acid at 25 °C between cross polarizers. The sample was first heated to 120 °C and then cooled slowly to 25 °C.

Lyotropic Liquid Crystalline Properties. It is known that some rigid poly(benzobisazole)s are able to form lyotropic liquid crystals. This processing potential has been exploited to obtain combination of mechanical properties in fibers and films. The formation of lyotropic mesophases was studied by preparing different concentration of polymer solutions in methanesulfonic acid (MSA). It was found that polymers **1a**−**c** exhibit lyotropic liquid crystal phases because of the more rigid main chain. To study the phase transition behavior, the polymer solutions were sandwiched between two microscope slides and the samples were allowed to stand in a desiccator. The lyotropic mesophases slowly formed in 5−6 h. The formation of the mesophase began at the critical concentration at which the solution became cloudy and birefringence was observed with an isotropic background. The critical concentration for the formation of mesophase is approximately 3−4 wt %. Figure 5 shows the polarized micrograph of polymer **1a** where a typical schlieren texture with disclination points of $^1/_2$ and 1 were observed. When the solution was heated above the clearing temperature and then cooled again, the birefrigence reappeared. A plot of clearing temperature versus solution concentration for polymers **1a**−**c** is shown in Figure 6. It can be seen that the clearing temperature of polymer **1c** (*trans*-PBT) is significantly higher than those of polymers **1a** and **1b** (*trans*- and *cis*-PBOs). The formation of lyotropic mesophases is strongly influenced by the flexibility of the polymer main chain. Polymers **2a**−**c** contain the 4,4′-substituted bipyridyl moieties, and their polymer solutions do not show any anisotropy because of the less rigid polymer main chain.

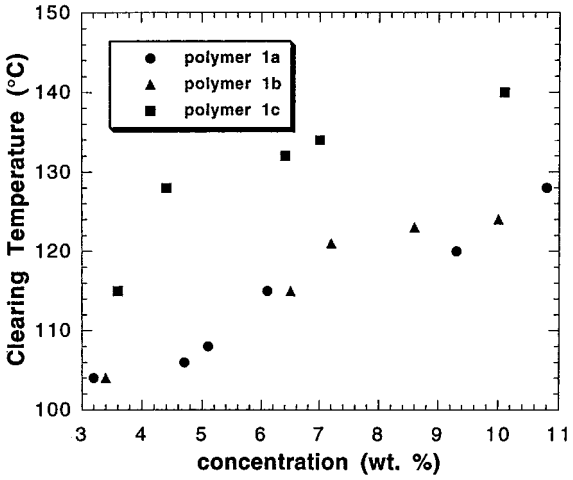

Figure 6. Plot of clearing temperature vs solution concentration for polymers **1a**−**c**.

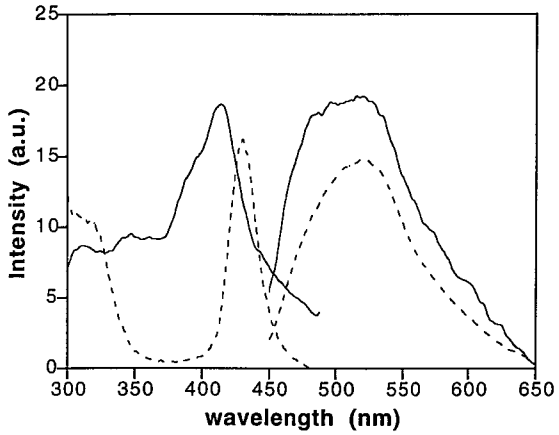

Figure 7. Excitation and emission spectra of model compounds **7a** (- - -) and **8a** (—) (excited at 380 nm, emission 515 nm).

Luminescent Properties. The emission and excitation spectra of model compounds **7a** and **8a** in formic acid solution are shown in Figure 7. When excited at 380 nm, both compounds showed an emission band at 450−650 nm assignable to the luminescence of the conjugated systems. For the ruthenium-containing complex **8a**, a shoulder was observed at ca. 570−590 nm. This is clearly due to the emission from the MLCT states of the ruthenium complexes. The excitation spectra of both compounds at 515 nm also show the peaks due to the absorption by the conjugated system. For polymer **1b** and its corresponding polymer metal complex **Ru**−**1b**, similar spectral features were observed (Figure 8). The emission peak at 530 nm and the shoulder at 580 nm are attributed to the emission from conjugated backbone and the MLCT states, respectively. These observations further prove the incorporation of the ruthenium bis(2,2′-bipyridyl) moiety into the polymer backbone.

Cyclic Voltammetry. The redox properties of model compounds **8a**−**d** are in general characterized by a single, primarily metal-centered oxidation and a series of reversible, one-electron ligand-centered reductions. The half-wave potentials of all of the redox processes exhibited by these metal complexes are summarized in Table 2. All four complexes have very similar oxidation potentials at approximately 1.41 V (vs Ag/AgCl), indicating that changing the ligands has very little effect

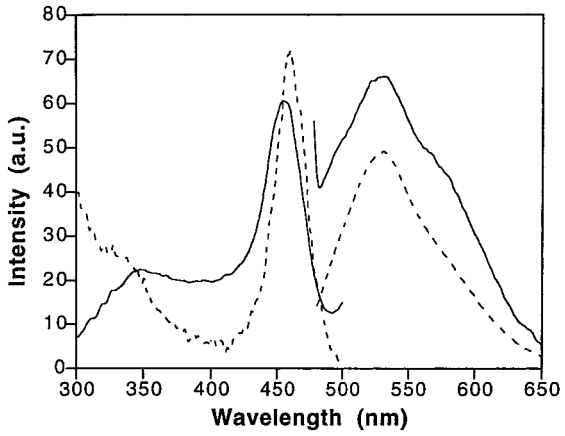

Figure 8. Excitation and emission spectra of polymer **1b** (- - -) and **Ru**−**1b** (—) (excited at 406 nm, emission 530 nm).

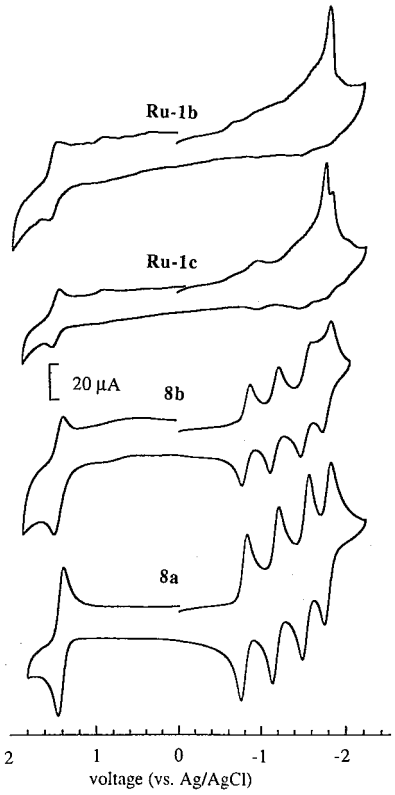

Figure 9. Cyclic voltammograms of model compounds **8a**,**b** and the polymer metal complexes **Ru**−**1b** and **Ru**−**1c** in acetonitrile with 0.1 M tetrabutylammonium hexafluorophosphate as the supporting electrolyte. Glassy carbon was used as the working electrode, and the scan rate was 100 mV/s.

on the $Ru^{3+/2+}$ couple.[19] In addition, the benzobisoxazole moieties also have little influence on the ligand-centered reduction processes, as both compounds **8a**,**b** demonstrate very similar reduction peaks. It should also be noted that the reduction potentials of complexes **8a**,**b** differ from **8c**,**d** by 0.15 V, with the 4,4′-substituted bipyridine being more difficult to reduce because of less extended electron delocalization. Figure 9 shows the cyclic voltammograms of model compounds **8a**,**b** and the polymer metal complexes **Ru**−**1b** and **Ru**−**1c**. The reversible metal-centered oxidation process can be observed clearly. Therefore, we expect that these metal-containing polymers may serve as hole-transporting materials. On the other hand, only one cathodic wave is observed at −1.65 V due to the reduction of the polymer backbone (the n-doping process). The irrevers-

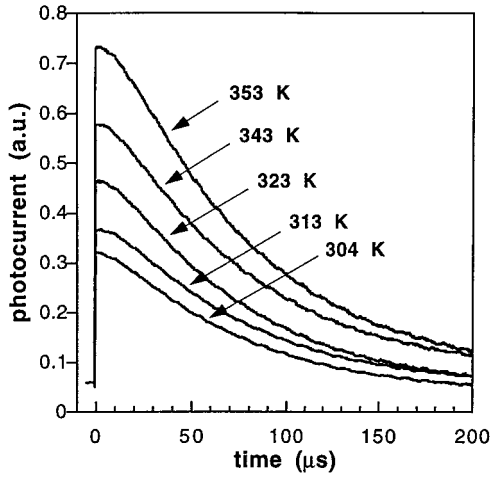

Figure 10. Transient photocurrent profile due to hole transport for polymer **Ru−1c** at different temperatures.

ibility may be associated with the charge trapping in the polymer during the doping process.

Charge Carrier Mobilities of the Polymers. Polymers with high charge carrier mobilities are of fundamental importance to the design and construction of advanced electronic devices. We have studied the charge carrier drift mobilities of the polymers before and after metal complex formation by conventional time-of-flight (TOF) experiments. In these experiments, the transient photocurrent generated by a laser pulse is monitored by using an oscilloscope. Figure 10 shows the transient photocurrent profile due to hole transport of polymer **Ru−1c**. The photocurrent pulse shows a featureless decay, and the transient time cannot be determined directly from the photocurrent trace. The transient time t_T is defined as the time when the leading part of the carrier distribution reaches the collecting electrode. The signals indicate a typical non-Gaussian carrier distribution which is usually found in disordered solid. The transient photocurrent is predicted by the equation

$$I(t) \propto \begin{cases} t^{-(1-\alpha)} & t < t_T \\ t^{-(1+\alpha)} & t < t_T \end{cases} \quad 0 < \alpha < 1$$

where α is the dispersion parameter.[20] The transit time and the hole mobility are defined by the intercept of the tangents approximating the current pulse at early and late times in the log I vs log t plot. Drift mobility μ was calculated by the equation $\mu = L/t_T E$, where L is the film thickness and E is the applied electric field. For polymers **1a−c**, the films casted from MSA solution broke down under high electric field because the solvent residue was difficult to remove. We then prepared the polymer films by casting from formic acid solution. The formic acid was removed by heating the polymer film at 90 °C in vacuo for 2 days. At room temperature, the hole and electron mobilities of these metal-free polymers are of the order of 10^{-6} cm^2 V^{-1} s^{-1}. The temperature and field-dependent mobility experiments were carried out on the polymer metal complexes **Ru−1b**,**c** because they formed the highest quality films. After the incorporation of ruthenium complexes to the polymer main chain, the mobilities increase by one to 2 orders of magnitude (Table 3), and they are both electric field and temperature dependent. The results clearly show that the ruthenium complexes are involved in the charge transport process.

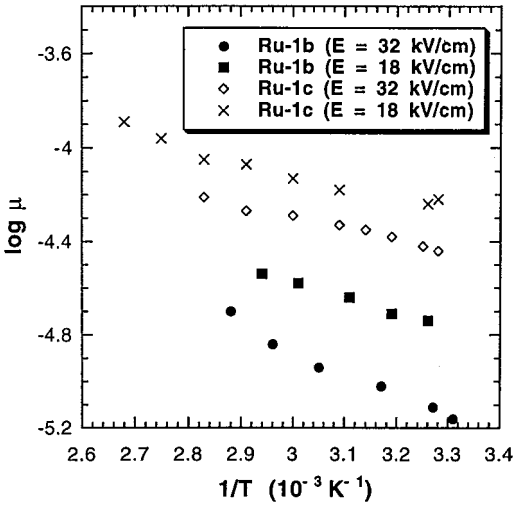

Figure 11. Temperature dependence of the hole mobility at E = 18 and 32 kV/cm for **Ru−1b** and **Ru−1c**.

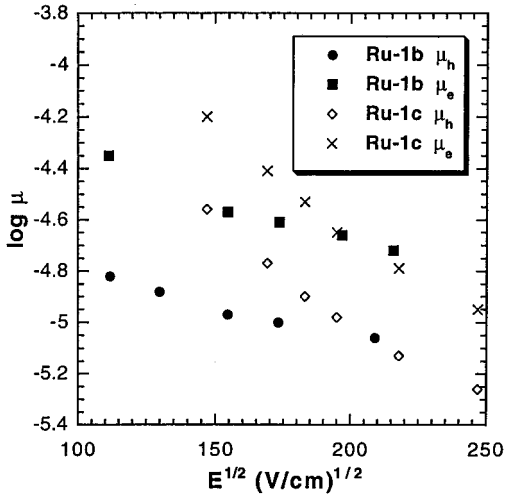

Figure 12. Field dependence of the electron and hole mobilities at T = 298 K for **Ru−1b** and **Ru−1c**.

Figure 11 shows the Arrhenius plot of the hole mobility for **Ru−1b** and **Ru−1c** under different applied electric field. The graph indicates a thermally activated charge migration process, and both polymers have similar value of activation energy in the range between 0.12 and 0.20 eV at E = 32 kV/cm. Figure 12 shows the plot of electron and hole mobilities for **Ru−1b** and **Ru−1c** at different field strength. The higher electron mobility indicates that the electron-withdrawing benzobisoxazole moieties facilitate the electron transport process. Moreover, both electron and hole mobilities decrease as the electric field strength increases. This is explained by the presence of off-diagonal disorder which is also observed in the charge transport of some organic disordered solids.[21]

Conclusions

A series of bipyridine-containing benzobisazole polymers were synthesized by condensation reaction between 2,2′-bipyridinecarboxylic acid and diaminobenzenediol in the presence of poly(phosphoric acid) as the condensing agent. These polymers exhibited extremely high thermal stabilities due to the rigid polymer main chain. Lyotropic liquid phases were observed when the polymers were dissolved in methanesulfonic acid. After the formation of metal complexes with the bis(2,2′-

bipyridyl)ruthenium(II) moiety, the electronic absorption, luminescence, and redox behavior of the resulting polymers were changed. The charge carrier mobilities of these polymer metal complexes were investigated by time-of-flight experiments. It was found that the drift mobilities were enhanced compared to the metal-free polymer by 1−2 orders of magnitude, indicating the participation of the metal complexes in the charge transport process.

Acknowledgment. We thank Prof. Vivian Yam and Dr. Wing Tak Wong for their assistance to the luminescence and CV measurements. This work was supported by the Research Grant Council of Hong Kong and by the Committee on Research and Conference Grants (University of Hong Kong). Partial financial support from the Hung Hing Ying Physical Science Research Fund and The Run Run Shaw/Leung Kau Kui Research and Teaching Endowment Fund is also acknowledged.

References and Notes

(1) (a) *Handbook of Conducting Polymers*; Skotheim, T. A., Ed.; Marcel Dekker Inc.: Basel, 1989. (b) *Organic Conductive Molecules and Polymers*, Nalwa, H. S., Ed.; John Wiley & Sons: West Sussex, U.K., 1997.

(2) (a) Wolfe, J. F. In *Encyclopedia of Polymer Science and technology*, 2nd ed.; Mark, H. F., Kroschmitz, J. I., Eds.; Wiley: New York, 1988; Vol. 11, pp 601−635. (b) *The Materials Science and Engineering of Rigid-Rod Polymers*; Adams, W. W., Edy, R. K., McLemore, D. E., Eds.; Symposium Proceedings Vol. 134; Materials Research Society: Pittsburgh, PA, 1989.

(3) (a) Jenekhe, S. A.; Osaheni, J. A. *Science* **1994**, *265*, 765. (b) Osaheni, J. A.; Jenekhe, S. A. *Macromolecules* **1994**, *27*, 739. (c) Osaheni, J. A.; Jenekhe, S. A.; Perlstein, J. *J. Phys. Chem.* **1994**, *98*, 12727. (d) Lefkowitz, S. M.; Roitman, D. B. *Polymer* **1994**, *35*, 1576. (e) Leugers, M. A.; Lefkowitz, S. M. *Polymer* **1994**, *35*, 4235.

(4) (a) Lee, C. Y.-C.; Swiatkiewiecz, J.; Prasad, P. N.; Mehata, R.; Bai, S. J. *Polymer* **1991**, *32*, 1195. (b) Dotrong, M.; Mehta, R.; Balchin, G. A.; Tomlinson, M.; Sinsky, M.; Lee, C. Y.-C. *J. Polym. Sci., Part A: Polym. Chem.* **1993**, *31*, 723.

(5) (a) Osaheni, J. A.; Jenekhe, S. A. *Macromolecules* **1993**, *26*, 4726. (b) Osaheni, J. A.; Jenekhe, S. A. *J. Am. Chem. Soc.* **1995**, *117*, 7389.

(6) (a) Wang, C. S.; Burkett, J. L.; Lee, C. Y.-C.; Arnold, F. E. *J. Polym. Sci., Polym. Phys. Ed.* **1993**, *31*, 1799. (b) Tan, L.-S.; Srinvasan, K. R.; Bai, S. J. *J. Polym. Sci., Part A: Polym. Chem.* **1997**, *35*, 1909.

(7) (a) Ng, W. Y.; Chan, W. K. *Adv. Mater.* **1997**, *9*, 716. (b) Chan, W. K.; Gong, X.; Ng, W. Y. *Appl. Phys. Lett.* **1997**, *71*, 2919. (c) Ng, P. K.; Gong, X.; Chan, W. K. *Macromol. Rapid Commun.* **1997**, *18*, 1009.

(8) (a) Kalyanasundaram, K. *Coord. Chem. Rev.* **1982**, *46*, 159. (b) Juris, A.; Balzani, V.; Barigelletti, F.; Campagna, S.; Belser, P.; Von Zelewsky, A. *Coord. Chem. Rev.* **1988**, *84*, 85.

(9) Lee, J.-K.; Yoo, D. S.; Handy, E. S.; Rubner, M. F. *Appl. Phys. Lett.* **1996**, *69*, 1.

(10) Peng, Z.; Gharavi, A. R.; Yu, L. *J. Am. Chem. Soc.* **1997**, *119*, 4622.

(11) Wang, B.; Wasielewski, M. R. *J. Am. Chem. Soc.* **1997**, *119*, 12.

(12) Yamamoto, T.; Maruyama, T.; Zhou, Z.-H.; Ito, T.; Fukuda, T.; Yoneda, Y.; Begum, F.; Ikeda, T.; Sasaki, S.; Takezoe, H.; Fukuda, A.; Kubota, K. *J. Am. Chem. Soc.* **1994**, *116*, 4832 and references therein.

(13) Bos, K. D.; Kraaijkamp, J. G.; Noltes, J. G. *Synth. Commun.* **1979**, *9*, 497.

(14) Inbasekaran, M.; Strom, R. *Org. Prep. Proc. Int.* **1991**, *23*, 447.

(15) Wolfe, J. F.; Loo, B. H.; Arnold, F. E. *Macromolcules* **1981**, *14*, 915.

(16) Sullivan, B. P.; Salmon, D. J.; Meyer, T. J. *Inorg. Chem.* **1978**, *17*, 3334.

(17) Peng, X.; Horowitz, G.; Fichou, D.; Garnier, F. *Appl. Phys. Lett.* **1990**, *57*, 2013.

(18) (a) Yagi, K.; Rivera-Castro, M. D. L.; Cedeno, R.; Inoue, Motomichi, *Inorg. Chim. Acta* **1987**, *131*, 273. (b) Yamamoto, T.; Maruyama, T.; Ikeda, T.; Sisido, M. *J. Chem. Soc., Chem. Commun.* **1990**, 1306. (c) Maruyama, T.; Kubota, K.; Yamamoto, T. *Macromolecules* **1993**, *26*, 4055. (d) Yamamoto, T.; Maruyama, T.; Zhou, Z.-H.; Ito, T.; Fukuda, T.; Yoneda, Y.; Begum, F.; Ikeda, T.; Sasaki, S.; Takezoe, H.; Fukuda, A.; Kubota, K. *J. Am. Chem. Soc.* **1994**, *116*, 4832. (e) Jessen, S. W.; Blatchford, J. W.; Lin, L.-B.; Gustafson, T. L.; Partee, J.; Shinar, J.; Fu, D.-K.; Marsella, M. J.; Swager, T. M.; MacDiarmid, A. G.; Epstein, A. J. *Synth. Met.* **1997**, *84*, 501.

(19) Elliott, C. M.; Hershenhart, E. J. *J. Am. Chem. Soc.* **1982**, *104*, 7519.

(20) (a) Scher, H.; Montroll, E. W. *Phys. Rev. B* **1975**, *12*, 2455. (b) Pfister, G.; Scher, H. *Adv. Phys.* **1972**, *43*, 943.

(21) (a) Borsenberger, P. M.; Pautmeier, L.; Bässler, H. *J. Chem. Phys.* **1991**, *94*, 5447. (b) Van der Auweraer, M.; De Schryver, F. C.; Borsenberger, P. M.; Bassler, H. *Adv. Mater.* **1994**, *6*, 199.

MA980381P